Applied Catalysis B: Environmental 217 (2017) 622–628

Contents lists available at ScienceDirect

Applied Catalysis B: Environmental

journal homepage: www.elsevier.com/locate/apcatb

Hexaazatriphenylene doped carbon nitrides—Biomimetic photocatalyst with superior oxidation power

Bogdan Kurpil[a], Aleksandr Savateev[a,*], Vasiliki Papaefthimiou[b], Spyridon Zafeiratos[b], Tobias Heil[a], Sibel Özenler[c], Dariya Dontsova[a], Markus Antonietti[a]

[a] Max-Planck Institute of Colloids and Interfaces, Department of Colloid Chemistry, Research Campus Golm, 14424 Potsdam, Germany
[b] ICPEES, Institut de Chimie et des Procédés pour l'Energie, l'Environnement et la Santé, UMR 7515 CNRS/Université de Strasbourg, 25 rue Becquerel, 67087 Strasbourg cedex, France
[c] Türkisch-Deutsche Universität, Merkez, Şahinkaya Cd. No:86, 34820 Beykoz/İstanbul, Turkey

ARTICLE INFO

Article history:
Received 21 April 2017
Received in revised form 11 June 2017
Accepted 13 June 2017
Available online 15 June 2017

Keywords:
Poly(heptazine imide)
Hexaazatriphenylene-hexacarbonitrile
Carbon nitride
Water oxidation
Water reduction

ABSTRACT

Pyrazine rings are a fundamental part of folic acid and flavine – cofactors that participate in natural electron transfer processes. Electron deficient carbon nitrides, more specifically poly(heptazine imides) (PHI), emulating the structure of these pyrazine based cofactors were synthesized polymerizing 3-amino-1,2,4-triazole-5-thiol with hexaazatriphenylene-hexacarbonitrile or hexaazatriphenylene-hexaamide at 550 °C in the eutectic mixture of KCl/LiCl. The role of hexaazatriphenylene units is 1) to create electron deficient acceptor sites in the structure of semiconductor; 2) widen the spectral coverage up to near infrared region. The significantly increased oxidative power of such doped PHI was demonstrated by running oxygen evolution from water, 0.59 μmol h^{-1}, under visible light irradiation in the absence of any metal co-catalyst.

1. Introduction

Visible light photocatalysts have experienced a strong renaissance over the past two decades, as they are envisioned to be used in clean energy production and to fight against pollutants [1,2]. Among metal-free photocatalysts a special place is taken by graphitic carbon nitride (g-CN), which is the most stable allotrope of carbon nitride and consists of tri-*s*-triazine rings as building units. This polymer can be synthesized via pyrolysis of cyanamide, [3], dicyandiamide [4], melamine [5] or urea derivatives [6–8], and was found efficient for photocatalytic splitting of water [9–12], hydrocarbon oxidation [13], carbon dioxide storage [14], and many other reactions.

A special subclass of carbon nitride materials, potassium poly(heptazine imides) (PHI) with a highly organized local structure were recently prepared by pyrolysis of 1,2,4-triazoles in eutectic mixture of KCl/LiCl [15]. Due to well-organized local packing, PHI has an unusually high (+2.54 eV) valence band potential. Because of the latter, PHI has a sufficiently high overpotential to run water oxidation (i.e. oxygen liberation) even without noble metal co-catalysts [16]. This observation was breaking a paradigm, as all other semiconductor photocatalysts were either unable to generate oxygen or relied on noble metal co-catalysts in laboratory experiments. Nevertheless, water oxidation readily occurs in natural photosynthesis in plant leaves. PHI thereby offers a promising foundation for onward modification through precursors copolymerization [7,17].

The difficulty of water oxidation is associated with the multielectron nature of this process and necessity to remove four electrons, four H^+, and to create a weak oxygen-oxygen bond [18]. One of the possibilities to simplify this process in organocatalytic fashion is to introduce neighboring pyrazine unit into the polymeric photocatalyst. Pyrazine is electrochemically reduced in acidic medium *via* two electron process giving 1,4-dihydropyrazine [19]. Such pyrazine-doped PHI can to our opinion mimic the behavior of typical redox cofactors, folic acid and flavine, to facilitate electron transfer. Hexaazatriphenylenes **2** and **3** (HAT) are redox active molecules which in principle are able to participate in multielectron transfer in a neighbor environment and could be introduced into carbon nitride using precursors co-polymerization approach (Fig. 1) [20,21].

Due to the strong electron accepting properties and three pyrazine units this compound potentially can accept up to six electrons [22–24]. HATs are thermally stable [25]. The six cyano groups

* Corresponding author.
E-mail address: oleksandr.savatieiev@mpikg.mpg.de (A. Savateev).

http://dx.doi.org/10.1016/j.apcatb.2017.06.036
0926-3373/

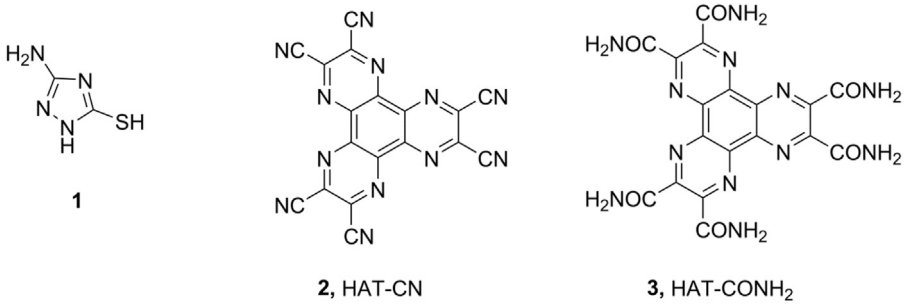

Fig. 1. Precursors for copolymerization: 3-Amino-1,2,4-triazole-5-thiol (**1**), HAT-CN (**2**) and HAT-$CONH_2$ (**3**).

could be used as addition sites to build the hexaazatriphenylene block into the semiconductor framework *via* nucleophilic addition and subsequent polymerization with nitrogen rich 3-Amino-1,2,4-triazole-5-thiol. Previously HATs have been successfully used as components of organic light-emitting diodes, [26–28], solar cells [29], cathode compounds in quasi-solid lithium cells [30] and as building blocks in covalent organic frameworks [31].

In the present work, hexaazatriphenylenehexacarbonitrile **2** and hexaazatriphenylenehexacarboxamide **3** were selected as co-monomers in a polymerization reaction with 3-amino-1,2,4-triazole-5-thiol **1** to obtain new modified PHIs with improved redox properties for multielectron processes, such as oxygen liberation.

2. Experimental section

2.1. Materials

3-Amino-1,2,4-triazol-5-thiol (≥98%) and triethanolamine (TEOA, 98%) was purchased from Alfa Aesar. Lithium chloride (≥99%) was purchased from Carl Roth; potassium chloride (≥99.5%) and hexachloroplatinic acid (H_2PtCl_6, 8 wt.% aqueous solution) were purchased from Sigma Aldrich.

2.2. Synthesis procedures

The synthesis of hexaazatriphenylene-hexacarbonitrile (HAT-CN) and hexaazatriphenylene-hexacarboxiamide (HAT-$CONH_2$) was carried out according to previously described method [32].

2.2.1. Hexaazatriphenylenehexacarbonitrile (HAT-CN)

Hexaketocyclohexane octahydrate (4 g, 12.6 mmol) and diaminomaleonitrile (10.88 g, 100.8 mmol) were refluxed in AcOH (150 mL) for 2 h. The hot black suspension was filtered off and washed with hot AcOH (3 × 25 mL) to give a black solid. The solid was suspended into 30% HNO_3 (60 mL) and heated at 100 °C for 3 h. The solid was refluxed in MeCN (400 mL) for 2 h, then solution was filtered, filtrate was evaporated in vacuo to give orange solid (2.4 g, yield 50%). ^{13}C NMR (DMSO-d_6, 100 MHz): δ 142.0, 135.8, 114.5.

2.2.2. Hexaazatriphenylenehexacarboxiamide (HAT-CONH2)

Hexaazatriphenylenehexacarbonitrile (1.2 g, 3.12 mmol) was mixed with 96% H_2SO_4 (30 mL). The solid slowly dissolved to give red solution wich was left to stir for 72 h at room temperature. The solution was cooled, poured into ice (200 g), obtained yellow suspension was filtered, precipitate was washed with water (3 × 50 mL) and acetone (3 × 50 mL) and dried in vacuo to give a yellow solid (1.1 g, yield 72%). ^1H NMR (DMSO-d_6, 400 MHz): δ 8.42 (br s, 1H), 7.98 (br s, 1H). 140.8. ^{13}C NMR (DMSO-d_6, 100 MHz): δ 166.6, 148.7, 140.8.

2.2.3. Modified potassium poly(heptazine imide) synthesis

Lithium chloride (2.25 g), potassium chloride (2.75 g) and mixture 1 g of 3-Amino-1,2,4-triazol-5-thiol and HAT-CN or HAT-$CONH_2$ in corresponding molar ratios (see Table S2) were ground together in a mortar. The weight ratio between lithium chloride and potassium chloride was 9:11 corresponding to their eutectic composition. Reaction mixtures were transferred into porcelain crucibles and covered with lids. Crucibles were placed in the oven and heated under constant nitrogen flow (15 L min^{-1}) and atmospheric pressure at a following temperature regime: heating from room temperature to 550 °C for 4 h, annealing at 550 °C for 4 h. After completion of the heating program, the crucibles were allowed to cool slowly to room temperature under nitrogen flow. The crude products were removed from the crucibles, washed with deionized water (100 mL) for 3 h in order to remove salts, then filtered, extensively washed with deionized water and dried in a vacuum oven (20 mbar) at 50 °C for 15 h.

3. Results and discussion

HAT-CN and HAT-$CONH_2$ were synthesized according to the procedures given in the literature [32]. The thermal stability of HAT-CN and HAT-$CONH_2$ were assessed by thermogravimetric analysis (TGA) (Fig. 2a). Thus, HAT-CN is stable up to 430 °C followed by 73% weight loss at 600 °C. In case of HAT-$CONH_2$ the first step in the range 25–100 °C is presumably due to the loss of water captured *via* hydrogen bonding with amide groups. The following mass decrease, up to 600 °C, nicely fits to the dehydration of carboxamide groups leading to carbonitrile recovery [33]. The multi electron redox nature of HAT-CN is revealed from the cyclic voltammetry curve (Fig. 2b). Peaks pairs 1/7, 2/6 and 3/5 form quasi reversible redox couples as their peak-to-peak separation, 159 mV, 147 mV and 205 mV respectively, exceed 57 mV, which is one of the requirements specified to electrochemically reversible process [34]. The band gap of hexanitrile **2** is 2.32 eV, while hexaamide **3**–2.61 eV as determined from their absorption spectra in DMSO (Fig. S1).

Both HAT-CN and HAT-$CONH_2$ have six nitrile/six amides groups, respectively. Each of these groups is able to react with nucleophiles, such as amino groups of triazole **1**. Therefore, multiples of the six-fold amount of triazole to HAT in co-monomer composition were selected to prepare modified PHIs (Table S1).

The assignment of the chemical structure of the products was done based on the results of elemental analysis (EA, EDS, XPS), Fourier transform infrared spectroscopy attenuated total reflectance (FTIR-ATR) and the identity of the powder X-ray diffraction (PXRD) patterns of the solids to the reported for PHI by us previously [15,16].

The elemental analysis data is summarized in Table S2. The C/N ratios range from 0.594 to 0.71 and correlates with the fraction of added HAT precursor. The potassium content in copolymerized samples is in the range 7.4–11.3 wt.%. i.e. composition agrees with the assumption of having potassium poly(heptazine imide) deriva-

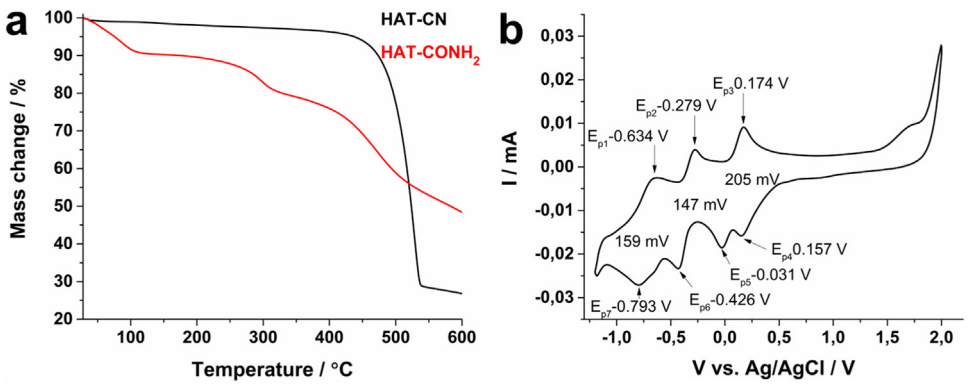

Fig. 2. a) TGA curves of HAT-CN and HAT-$CONH_2$ recorded under nitrogen flow at the heating rate of 10 K min^{-1}. b) CV curve of HAT-CN recorded at the sweep rate 100 mV s^{-1} in DCM ($5{\cdot}10^{-5}$ M).

tives. EDX mapping patterns of the C, N, K elements (Figs. S2–S7) are similar confirming that they belong to the same phase.

The FTIR spectra of the synthesized materials are similar to the reported by us previously implying that the main contribution to vibration bands come from heptazine rings (Fig. S8), [15,16], e.g. the absorption peak at 800 cm^{-1}, corresponding to deformation vibration of tri-*s*-triazine system, and the one at 985 cm^{-1} due to symmetric vibrations of NC_2 bonds in metal–NC_2 groups [35]. The broad peak at 2500–3600 cm^{-1} is due to the presence of uncondensed amino groups and HO-surface groups [36].

XPS spectra of the synthesized materials are similar to each other (Figs. 3 a,b, S9) [15]. Deconvoluted C *1s* core level spectrum of PH-CN-2 shows three components (Fig. 3a). The peak with the binding energy 288.5 eV is related to the quaternary (CN_3) carbon atoms in the heterocycles. The peak at 286.7 eV is due to the hydroxylated surface carbon atoms while the one at 285.0 eV corresponds to adventitious carbon atoms and sp^2 hybridized carbon atoms of C═C bonds in HAT unit. After deconvolution, the N *1s* spectrum shows the peak at 403.9 eV that is due to the presence of N—O bonds, formed presumably during product aqueous workup. The peaks at 400.9 eV and 398.6 eV correspond to various NHx groups and C—N═C nitrogen atoms in heterocycles, respectively (Fig. 3b). The peak at 396.7 eV is related to the negatively charged C—$N^{\ominus}$—C groups.

The presence of the diffraction peaks at 8°, (100) plane, in all PXRD patterns due to in-plane repeating motif and 27–28°, (220) plane, due to the stacked structure again indicate the formation of PHI network (Fig. 3c) [15,16,37]. However, the intensity of the peak at 8° in all co-polymerized products is lower compared to the reference material, suggesting that introduction of HAT units expectedly perturbs the in-plane periodicity. The absence of the diffraction peaks, additional to 8 and 27°, suggested that HAT units are rather distributed randomly over the polymer network than forming the phase separated structure, as schematically depicted in Fig. 3d.

The morphology of the synthesized materials depends on the co-monomer fraction (Fig. 4). The addition of 2 wt.% HAT-CN did not affect the morphology of the final material, as it is similar to the observed previously for pure PHI, represented by 200–300 nm long rods (Fig. 4a) [15,16]. When HAT-CN content was increased to 4 wt.%, the rods size decreased (Fig. 4b). The morphology of PH-AM-1 (Fig. 4c) is similar to PH-CN-4 despite the lower co-monomer content. Higher content of amide **3** in the starting mixture naturally affects the polymer morphology even stronger – in case of PH-AM-2 it is represented by sheets having a rather smooth surface (Fig. 4d).

Highly organized structure of PH-CN-2 is clearly seen from aberration corrected high resolution transmission electron microscopy (AC-HRTEM) images (Fig. 5a,b). Thus, poly(heptazine imide) exhibits stacked structure, similar to g-CN, with the distance between layers 0.32 nm. This value matches well with the diffraction peak observed in PXRD pattern at 27.2 °. K^+ ions of PH-CN-2 are arranged in lines with the distance 0.94 nm between the neighboring threads. This repeating motif is also seen as a diffraction peak at 8.15 ° (Fig. 3d) [38]. The electron energy loss (EEL) spectrum (Fig. 5c) displays carbon *K*-edge represented by a very intense 1s-π* at 287.0 eV and σ* at 294.0 eV that overlaps with potassium peaks. The inset on Fig. 5c shows potassium peak composed of transitions to the $2p_{3/2}$ and $2p_{1/2}$ orbitals of the *L*-edge with the energies 297.5 eV and 300.0 eV, respectively. All values are shifted ca. 3 eV to higher energies compared to the literature data [39]. This phenomenon is not uncommon and could be caused by chemical shift [40]. AC-HRTEM images of PH-CN-4 and PH-CN-0.5 with EEL spectra as insets are shown in Fig. 5d,e respectively.

From the N_2 sorption isotherms (Fig. S10) we have concluded that the materials do not possess distinct porosity. However, PH-AM-1 and PH-AM-2 demonstrate maximum pore volume of 0.12 $cm^3\ g^{-1}$ and 0.20 $cm^3\ g^{-1}$ at pore diameter 4 nm. Surface areas of the samples modified with HAT-CN are in the range 19–27 $m^2\ g^{-1}$ (Table S1) which is comparable to the reference sample (23 $m^2\ g^{-1}$). At the same time, HAT-$CONH_2$ modified PHI have larger surface area of 66–100 $m^2\ g^{-1}$, quantifying their tendency to form delaminated products, presumably as a consequence of higher polarity of amides and water elimination [41].

In visible light absorption spectra of the materials two main peaks at 460–475 nm and 500–525 nm are present (Fig. 6a), which are usually assigned to π-π* and n-π* transitions [42–44]. The HAT moiety might activate n-π* transitions *via* defects and deviations of the ring units from trigonal symmetry [45,46]. The effect becomes more pronounced when fraction of HAT co-monomer increases. HAT-CN has a larger effect on those electronic effects than HAT-$CONH_2$, i.e. PH-CN-2 absorbs a larger fraction of the light with the wavelength >600 nm than PH-AM-2, despite they were obtained using equal relative amounts of HAT precursor. Semiconductors optical bandgaps (BG) were determined using Tauc plots, and they range from 1.55 to 1.92 eV (Table S1). Generally, optical band gaps of the materials with higher co-monomer content are narrower. It indicates that addition of hexaazatriphenylene co-monomer produces material with a higher conjugation of π-system compared to the reference PHI. At the same time, optical band gaps of PH-CN-2 and PH-AM-2 are 1.65 eV and 1.80 eV respectively implying that nitrile **2** favors the formation of the polymer structure even with higher degree of π-conjugation. This is presumably due to higher reactivity of CN group compared to $C(O)NH_2$ at earlier stages of the polycondensation providing a material with more anchoring points between the hexaazatriphenylene unit and the PHIK network.

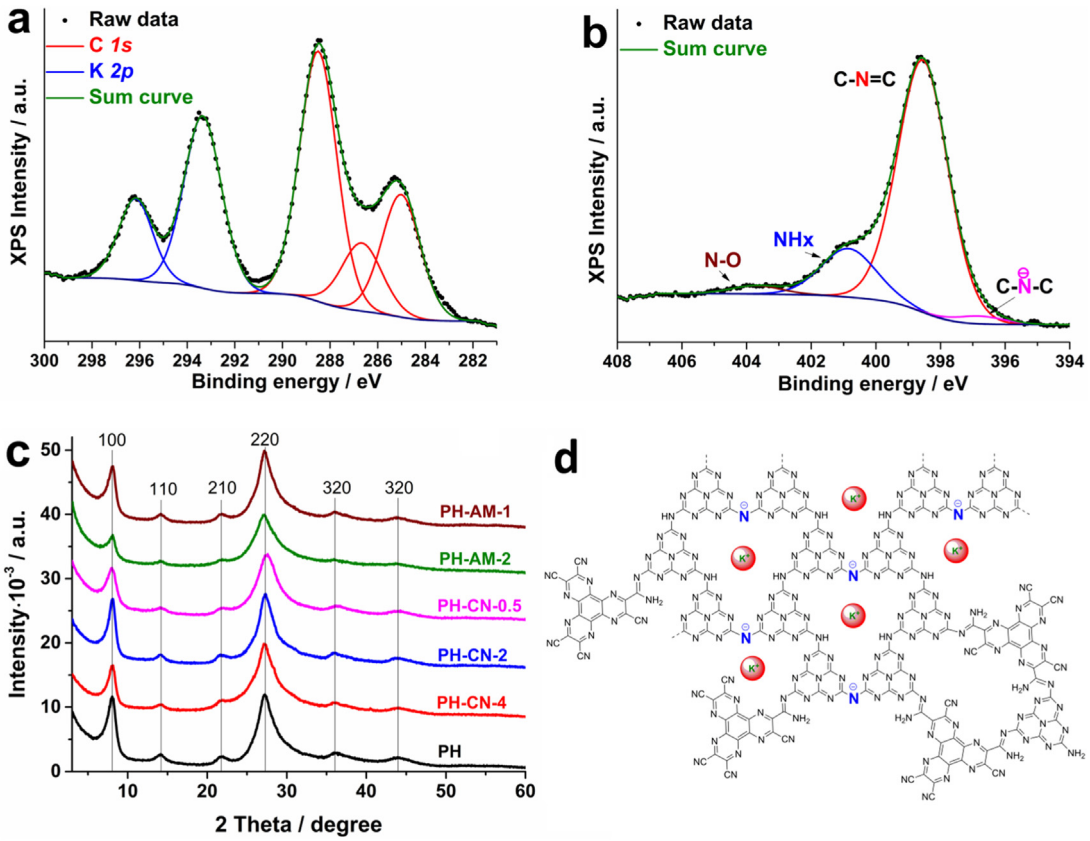

Fig. 3. Deconvoluted C *1s* and K *2p* (a) and N 1s (b) XPS spectra of PH-CN-2; PXRD patterns with Miller indices (c) of PH, PH-CN and PH-AM and the proposed structure of the materials (d).

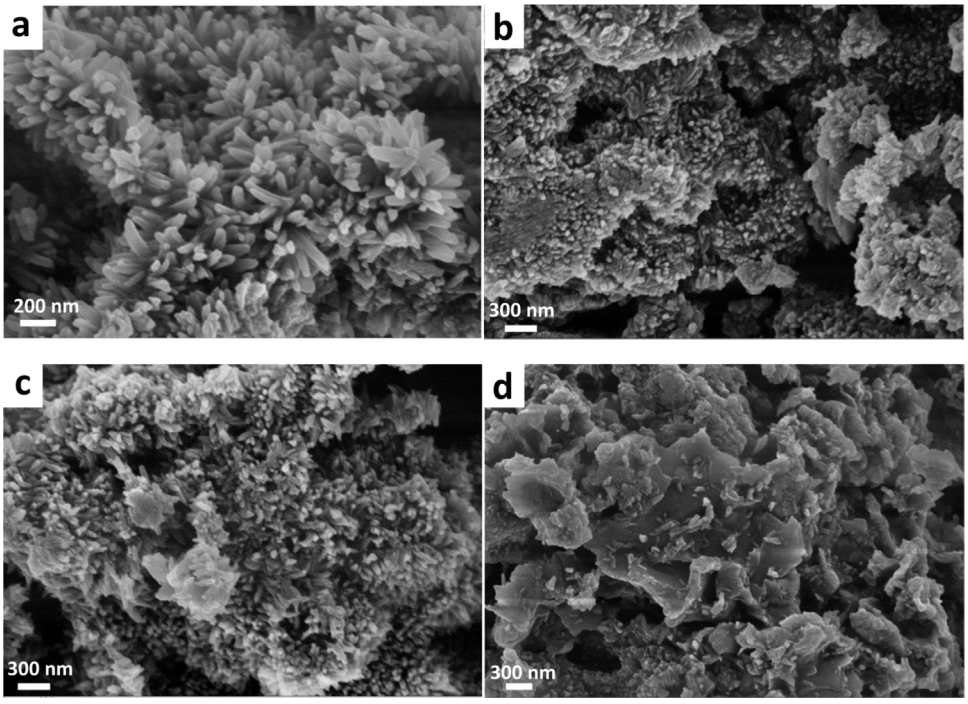

Fig. 4. SEM images of PH-CN-2 (a), PH-CN-4 (b), PH-AM-1 (c) and PH-AM-2 (d).

Ultraviolet photoelectron spectroscopy (UPS) was used to determine valence band maximum (VBM) of the materials (Fig. 6b, Table S1). The values are normalized versus vacuum energy. The VBM of the reference, PH, material is 2.1 eV, while the one of the modified semiconductor, PH-CN-2, lies at 2.6 eV. Modification of PHIK with HAT units indeed lowers valence band position of the material, ca. 0.5 eV, when compared to pure poly(heptazine imide). The VBM values of all materials comprising poly(heptazine imide) are

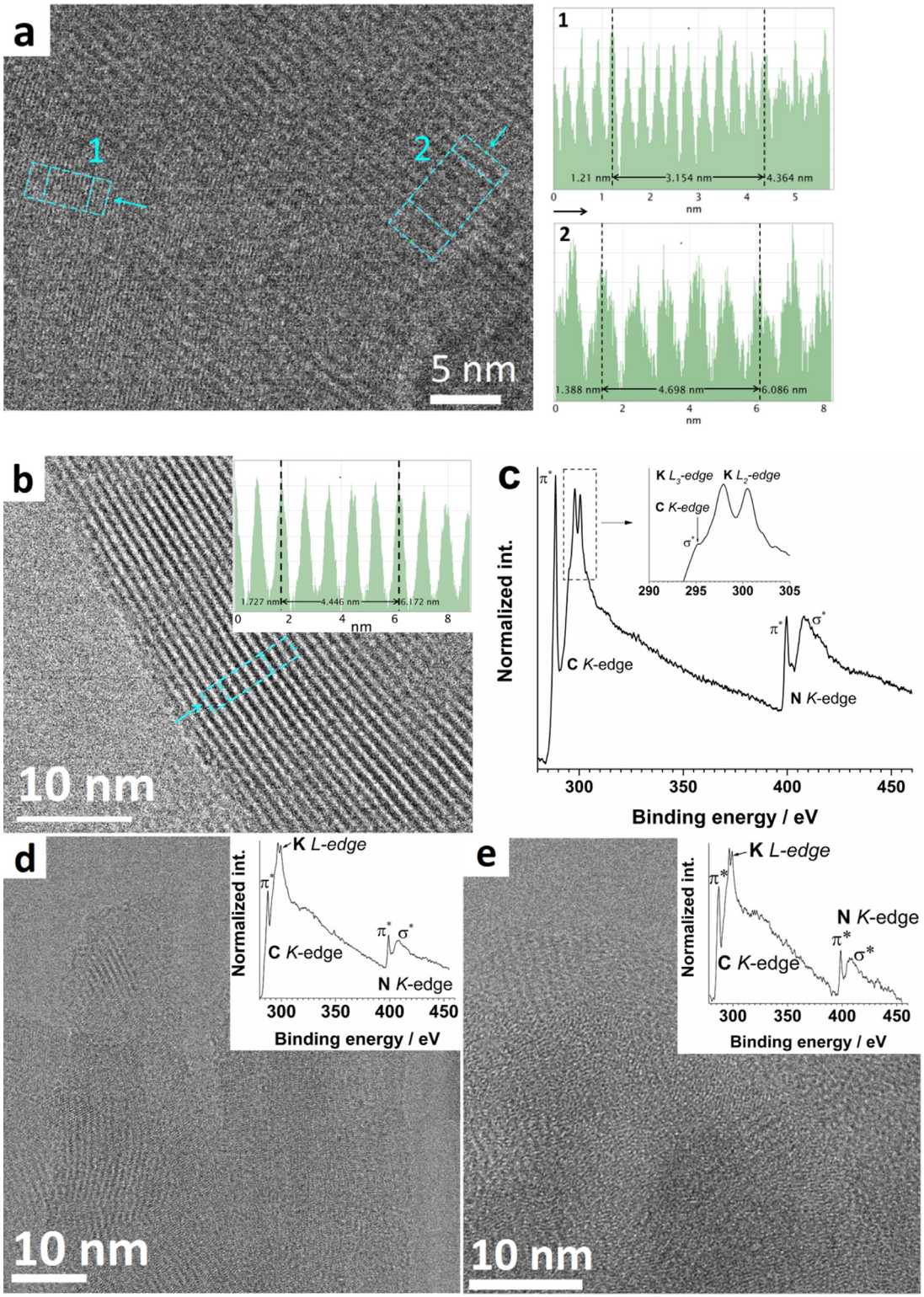

Fig. 5. (a,b) AC-HRTEM image of PH-CN-2 with the profiles of the selected areas. The direction of view is shown by arrows. (c) EEL spectrum of PH-CN-2. (d) AC-HRTEM image of PH-CN-4 with EEL spectrum as inset. (e) AC-HRTEM image of PH-CN-0.5 with EEL spectrum as inset.

significantly more positive than that of pristine graphitic carbon nitride, 1.38 eV. [47],

The intensity of photoluminescence of all modified PHIs, except PH-CN-0.5, is slightly lower (Fig. S11) than of the reference sample. This feature is attributed by the presence of the hexaazatriphenylene moieties in the polymer structure acting as an electron acceptor that binds the photoexcited electrons to local electron deficient states, diminishing recombination with the generated holes. A similar positive effect is known from conjugated donor-acceptor (D-A) polymers for organic photovoltaics which simplify exciton dissociation [48]. All modified PHIs showed lower internal quantum efficiency (0.108-0.078%) compared to the reference PH sample (0.15%) (Table S1). These data support that HAT units

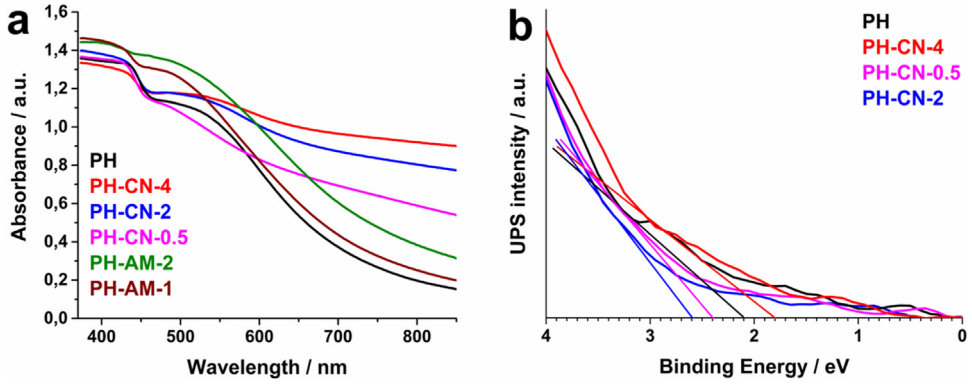

Fig. 6. Diffuse reflectance UV–vis (a) and UPS (b) spectra of the synthesized materials.

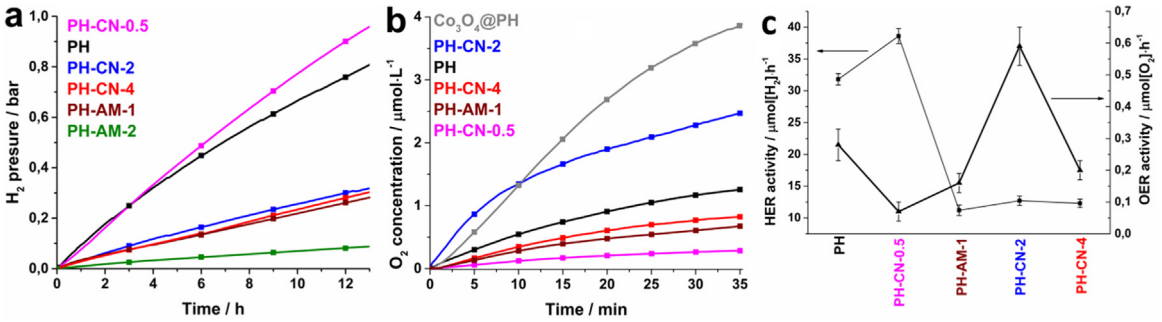

Fig. 7. (a) Time dependent HER profiles. TEOA was used as a sacrificial hole scavenger, co-catalyst – photodeposited Pt nanoparticles. (b) Time dependent OER profiles. $AgNO_3$ was used as a sacrificial electron scavenger. Light source – white LED (90 mW cm^{-2}). (c) Summary of structure-activity correlation.

decrease the rate of photogenerated charge carriers recombination *via* fluorescence.

In order to assess the impact of doping onto PHI photocatalyst performance, standardized hydrogen evolution reactions (HER) were performed (Table S1, Fig. 7a) [49]. PH-CN-0.5 demonstrated HER activity of 38.6 μmol $H_2 \cdot h^{-1}$, which is slightly higher when compared to the reference PH material, 31.8 μmol $H_2 \cdot h^{-1}$ and can be related to a higher surface area and wider spectral coverage. Under the identical conditions the benchmark mesoporous graphitic carbon nitride (mpg-CN) showed activity of 16.8 μmol $H_2 \cdot h^{-1}$ (Fig. S12). Notably, the activities of all other samples with higher doping degree are significantly lower compared to the reference. As a case, PH-AM-2 having the highest surface area of 100 $m^2 \cdot g^{-1}$ among studied materials exposed an activity of only 4.4 μmol $H_2 \cdot h^{-1}$. The improved electron-accepting properties of the obtained polymers obviously disfavor the transfer of electrons from the semiconductor to the Pt co-catalyst.

The strong electronegative nature of HAT-doped PHIs, however, was turned into advantage in oxygen evolution reaction (OER) under visible light irradiation. Even in the absence of any metal co-catalyst, the activity of PH-CN-2 was 2 times higher than the reference material (Fig. 7b, Table S1). The reasons for this improvement might be manifold: the strong electron accepting HAT units into PHIK network may increase electron-deficient nature of the photocatalyst as a whole and consequently improves the overpotentials for photo-induced oxidation processes. This is in agreement with the more positive VB potential determined by UPS. Other reasons might be an improved uptake of the four protons (with the electrons) by HAT units, thus avoiding local pH effects. Finally, much higher activity of PH-CN-2 in OER could be rationalized by highly organized local structures as it is clearly seen from EEL spectrum (Fig. 5c) [50]. High organization on the micro level originates, apparently, from the stoichiometric composition of the reaction mixture used to prepare photocatalyst. Thus, 2 wt.% of HAT in the starting precursors mixture corresponds the ratio between HAT **2** and 3-Amino-1,2,4-triazole-5-thiol **1** of 1:48.

Despite PHI itself is efficient to oxidize water, its performance can be improved even further using Co_3O_4 as a co-catalyst [51]. In this case the activity of the copolymer is 3 times higher compared to bare PH, 0.88 versus 0.28 μmol $O_2 \cdot h^{-1}$.

As the result, introduction of the electron deficient HAT units improves the performance of the photocatalyst in OER (Fig. 7c). Nevertheless, the activity of all HAT-doped poly(heptazine imides) in HER is either higher or comparable to mpg-CN, which however shows no activity in OER under identical conditions (Fig. S12b). Apparently, the maximum activity in OER is observed when material is doped with 2 wt.% of HAT. PH-CN-2 demonstrates significantly higher activity in OER compared to bare PH, while its activity still remains comparable to mpg-CN. On the other hand, materials with HAT doping above 0.5 wt.% exhibits nearly the same activity in HER. The photocatalytic reactions presented above prove high potential of HAT-modified PHIs for application in different kind photooxidation reactions under visible light [52].

4. Conclusion

To improve artificial photosynthesis, monomers mimicking redox active biological cofactors were introduced into the framework of the polymeric carbon nitride semiconductor, more specifically poly(heptazine imide). The modification with such acceptors was indeed found very efficient to obtain electron deficient semiconductors. Hexaazatriphenylene-hexacarbonitrile and hexaazatriphenylene-hexaamide were used as co-monomers, and even tiny amounts of HAT-$CONH_2$ altered the morphology and increased the specific surface area of the final material up to 100 $m^2\ g^{-1}$. All HAT-CN doped PHIs consequently demonstrated a higher activity in the photochemical liberation of oxygen from water, which is driven by the holes located at the framework. The

photocatalyst activity in OER depends on the ratio between precursors. The highest activity, 0.59 μmol h^{-1} versus 0.28 μmol h^{-1} for the reference, was observed for the material prepared from forty eight 3-Amino-1,2,4-triazole-5-thiol molecules per one HAT unit. The rate of oxygen evolution could be increased up to 0.88 μmol h^{-1} using cobalt oxide co-catalyst. All samples showed photocatalytic activity in hydrogen evolution reaction. The activities are generally lower compared to the reference poly(heptazine imide), which take as an evidence of the electron deficient nature of the overall framework – the electrons prefer to be localized along the HAT units.

Acknowledgements

The authors gratefully acknowledge Deutsche Forschungsgemeinschaft (grant number DFG-An 156 13-1) and Max Planck Society for providing financial support to make this work possible.

Appendix A. Supplementary data

Supplementary data associated with this article can be found, in the online version, at 10.1016/j.apcatb.2017.06.036.

References

[1] W. Jiang, W. Luo, J. Wang, M. Zhang, Y. Zhu, J. Photochem. Photobiol. C 28 (2016) 87–115.
[2] G. Mamba, A.K. Mishra, Appl. Catal. B 198 (2016) 347–377.
[3] K. Maeda, X. Wang, Y. Nishihara, D. Lu, M. Antonietti, K. Domen, J. Phys. Chem. C 113 (2009) 4940–4947.
[4] H. Ji, F. Chang, X. Hu, W. Qin, J. Shen, Chem. Eng. J. 218 (2013) 183–190.
[5] S.C. Yan, Z.S. Li, Z.G. Zou, Langmuir 25 (2009) 10397–10401.
[6] J. Liu, T. Zhang, Z. Wang, G. Dawson, W. Chen, J. Mater. Chem. 21 (2011) 14398–14401.
[7] G. Zhang, X. Wang, J. Catal. 307 (2013) 246–253.
[8] Y. Cui, G. Zhang, Z. Lin, X. Wang, Appl. Catal. B 181 (2016) 413–419.
[9] G. Zhang, Z.-A. Lan, X. Wang, Angew. Chem. Int. Ed. 55 (2016) 15712–15727.
[10] G. Zhang, Z.-A. Lan, L. Lin, S. Lin, X. Wang, Chem. Sci. 7 (2016) 3062–3066.
[11] G. Zhang, S. Zang, Z.-A. Lan, C. Huang, G. Li, X. Wang, J. Mater. Chem. A 3 (2015) 17946–17950.
[12] Y. Wang, H. Wang, F. Chen, F. Cao, X. Zhao, S. Meng, Y. Cui, Appl. Catal. B 206 (2017) 417–425.
[13] Y. Wang, J. Zhang, X. Wang, M. Antonietti, H. Li, Angew. Chem. 122 (2010) 3428–3431.
[14] Q. Li, Jianping Yang, D. Feng, Z. Wu, Q. Wu, S.S. Park, C.-S. Ha, D. Zhao, Nano Res. 3 (2010) 632–642.
[15] D. Dontsova, S. Pronkin, M. Wehle, Z. Chen, C. Fettkenhauer, G. Clavel, M. Antonietti, Chem. Mater. 27 (2015) 5170–5179.
[16] A. Savateev, S. Pronkin, J.D. Epping, M. Willinger, C. Wolff, D. Neher, M. Antonietti, D. Dontsova, ChemCatChem (2017) 167–174.
[17] Z. Chen, S. Pronkin, T.-P. Fellinger, K. Kailasam, G. Vilé, D. Albani, F. Krumeich, R. Leary, J. Barnard, J.M. Thomas, J. Pérez-Ramírez, M. Antonietti, D. Dontsova, ACS Nano 10 (2016) 3166–3175.
[18] T.A. Betley, Q. Wu, T.V. Voorhis, D.G. Nocera, Inorg. Chem. 47 (2008) 1849–1861.
[19] L.N. Klatt, R.L. Rouseff, J. Am. Chem. Soc. 94 (1972) 7295–7304.
[20] J. Zhang, X. Chen, K. Takanabe, K. Maeda, K. Domen, J.D. Epping, X. Fu, M. Antonietti, X. Wang, Angew. Chem. 49 (2010) 441–444.
[21] J. Zhang, G. Zhang, X. Chen, S. Lin, L. Möhlmann, G. Dołęga, G. Lipner, M. Antonietti, S. Blechert, X. Wang, Angew. Chem. 51 (2012) 3183–3187.
[22] V. Lemaur, D.A.d.S. Filho, V. Coropceanu, M. Lehmann, Y. Geerts, J. Piris, M.G. Debije, A.M.v.d. Craats, K. Senthilkumar, L.D.A. Siebbeles, J.M. Warman, J.-L. Brédas, J. Cornil, J. Am. Chem. Soc. 126 (2004) 3271–3279.
[23] B.R. Kaafarani, T. Kondo, J. Yu, Q. Zhang, D. Dattilo, C. Risko, S.C. Jones, S. Barlow, B. Domercq, F. Amy, A. Kahn, J.-L. Brédas, B. Kippelen, S.R. Marder, J. Am. Chem. Soc. 127 (2005) 16358–16359.
[24] M. Lehmann, G. Kestemont, R.G. Aspe, C. Buess-Herman, M.H.J. Koch, M.G. Debije, J. Piris, M.P.d. Haas, J.M. Warman, M.D. Watson, V. Lemaur, J. Cornil, Y.H. Geerts, R. Gearba, D.A. Ivanov, Chem. Eur. J. 11 (2005) 3349–3362.
[25] M.M. Oliva, A. Riaño, I. Arrechea-Marcos, M.M. Ramos, R. Gómez, M. Algarra, R.P. Ortiz, J.T.L. Navarrete, J.L. Segura, J. Casado, J. Phys. Chem. C 120 (2016) 23276–23285.
[26] E. Najafabadi, K.A. Knauer, W. Haske, B. Kippelen, Org. Electron. 14 (2013) 1271–1275.
[27] S.H. Cho, S.W. Pyo, M.C. Suh, Synth. Met. 162 (2012) 402–405.
[28] B.B. Diouf, W.S. Jeon, J.S. Park, J.W. Choi, Y.H. Son, D.C. Lim, Y.J. Doh, J.H. Kwon, Synth. Met. 161 (2011) 2087–2091.
[29] C. Falkenberg, S. Olthof, R. Rieger, M. Baumgarten, K. Muellen, K. Leo, M. Riede, Sol. Energy Mater. Sol. Cells 95 (2011).
[30] Y. Hanyu, T. Sugimoto, Y. Ganbe, A. Masuda, I. Honma, J. Electrochem. Soc. 161 (2014) A6–A9.
[31] S.-Q. Xu, T.-G. Zhan, Q. Wen, Z.-F. Pang, X. Zhao, ACS Macro Lett. 5 (2016) 99–102.
[32] J.T. Rademacher, K. Kanakarajan, A.W. Czarnik, Synthesis 4 (1994) 378–380.
[33] N.K. Bhattacharyya, S. Jha, Sangeeta Jha, T.Y. Bhutia, G. Adhikary, Int. J. Chem. Appl. 4 (2012) 295–304.
[34] D.A.C. Brownson, C.E. Banks, The Handbook of Graphene Electrochemistry, Springer-Verlag, London, 2014.
[35] D.C. Bradley, M.H. Gitlitz, J. Chem. Soc. A (1969) 980–984.
[36] P. Larkin, IR and Raman Spectra-Structure Correlations: Characteristic Group Frequencies, Infrared and Raman Spectroscopy Principles and Spectral Interpretation, Elseiver, 2011.
[37] Z. Chen, A. Savateev, S. Pronkin, V. Papaefthimiou, C. Wolff, M.G. Willinger, E. Willinger, D. Neher, M. Antonietti, D. Dontsova, Adv. Mater. (2017), http://dx.doi.org/10.1002/adma.201700555.
[38] A. Savateev, S. Pronkin, M. Willinger, M. Antonietti, D. Dontsova, Chem.—Asian J. (2017), http://dx.doi.org/10.1002/asia.201700209.
[39] M. Cardona, L. Ley, Photoemission in Solids I: General Principles, Springer-Verlag, Berlin, 1978.
[40] C. Richter, L. Menon, Energy Environ. Sci. 3 (2010) 427–433.
[41] Y. Zhang, J. Liu, G. Wu, W. Chen, Nanoscale 4 (2012) 5300–5303.
[42] V.N. Khabashesku, J.L. Zimmerman, J.L. Margrave, Chem. Mater. 12 (2000) 3264–3270.
[43] J.Z. Yingai Li, Q. Wang, Y. Jin, D. Huang, Q. Cui, G. Zou, J. Phys. Chem. B 114 (2010) 9429–9434.
[44] A.B. Jorge, D.J. Martin, M.T.S. Dhanoa, A.S. Rahman, N. Makwana, J. Tang, A. Sella, F. Corà, S. Firth, J.A. Darr, P.F. McMillan, J. Phys. Chem. C 117 (2013) 7178–7185.
[45] Y. Chen, B. Wang, S. Lin, Y. Zhang, X. Wang, J. Phys. Chem. C 118 (2014) 29981–29989.
[46] M. Deifallah, P.F. McMillan, F. Corà, J. Phys. Chem. C 112 (2008) 5447–5453.
[47] L. Ma, H. Fan, M. Li, H. Tian, J. Fang, G. Dong, J. Mater. Chem. A 3 (2015) 22404–22412.
[48] R.S. Kularatne, H.D. Magurudeniya, P. Sista, M.C. Biewer, M.C. Stefan, J. Polym. Sci. Part A: Polym. Chem. 51 (2013) 743–768.
[49] M. Schwarze, D. Stellmach, M. Schröder, K. Kailasam, R. Reske, A. Thomas, R. Schomäcker, Phys. Chem. Chem. Phys. 15 (2013) 3466–3472.
[50] A. Savateev, S. Pronkin, J.D. Epping, M.G. Willinger, M. Antonietti, D. Dontsova, J. Mater. Chem. A 5 (2017) 8394–8401.
[51] J. Zhang, M. Grzelczak, Y. Hou, K. Maeda, K. Domen, X. Fu, M. Antonietti, X. Wang, Chem. Sci. 3 (2012) 443–446.
[52] A. Savateev, D. Dontsova, B. Kurpil, M. Antonietti, J. Catal. 350 (2017) 203–211.